BL-8B/ 2013G040

Phase transformation mechanism from ferrihydrite to hematite with particle size effect

Atsushi Kyono[1,*] and Yuki Nishimiya[2]
[1]University of Tsukuba, Tsukuba 305-8572, Japan
[2] National Institute for Materials Science, Tsukuba, Ibaraki, 305-0047, Japan

1 Introduction

Iron oxides and oxyhydroxides with a broad particle size distribution from nanoparticles to microparticles play an important role in iron cycling in the environment. Ferrihydrite is a poorly crystalline nanomineral that occurs widely in near-surface environments such as livers, lakes, hot and cold springs, water wells, ground water, soils, podsols, and mine drainage [1]. Because the ferrihydrite has an extremely large surface area and strong affinity for widely various metal ions, it functions as a metal sorbent and repository of toxic contaminations such as As, Cd, Pb, Zn, Cu, and [2-6]. The ferrihydrite is formed as an immediate precipitate by rapid polymerization and nucleation of hydrolyzed ferric iron [7]. Because of its thermodynamic instability, however, the ferrihydrite is readily transformed with time into more crystalline iron oxides and oxyhydroxides such as hematite (α-Fe_2O_3) and goethite (α-FeOOH) [7-9].

The ferrihydrite structure has been the subject of intense research for the two last decades [10-13]. A new structural model with about 20% tetrahedrally coordinated Fe atoms in the structure was proposed by Michel et al. [13] using an atomic pair distribution function (PDF) analysis derived from synchrotron-based total X-ray scattering data. This model strongly contradicts not only the previously accepted structural model that all Fe atoms are octahedrally coordinated to oxygen atoms [12], but also with X-ray diffraction patterns measured from so-called 6-line ferrihydrite [14-15]. Therefore, the presence of tetrahedrally coordinated Fe atom in the ferrihydrite structure has been a matter of considerable debate [17-20]. Recent reports of high-quality XANES and EXAFS experiments are apparently supportive of the model proposed by Michel et al. [13], although some disagreement is apparent in relation to the amount of tetrahedral Fe atoms [21-23].

For this study, we investigate the phase transformation mechanism of the 6-line ferrihydrite to hematite with synchrotron X-ray scattering technique and the PDF method. The results provide a reasonable explanation for the aggregation-induced phase transformation, which causes a change of coordination environment from tetrahedrally coordinated Fe atoms to octahedral coordination.

2 Experiment

Samples of the 6-line ferrihydrite were prepared by modification of the method described by Schwertmann and Cornell [1]. First, 150 mg of $Fe(NO_3)_3 \cdot 9H_2O$ were dissolved in 15 ml of distilled water. Then the solution was neutralized with NaOH. Second, the solution was kept at 75 ^oC for 10 min, 60 min, 90 min, 120 min, 4 h, 6 h, 12 h, and 24 h. After that heating stage, the solution was cooled rapidly by plunging into ice water. The solution was subsequently transferred to a dialysis tube and dialyzed for three days with daily replacement of the water. The suspension was then precipitated by adding n-butanol to the solution. Precipitate extracted with a pipette was finally dried overnight at room temperature in a clean draft chamber.

Suspended samples were dropped onto carbon-coated copper TEM grids. The liquid was allowed to evaporate from the grid, leaving a precipitate adhered to the grids. High-resolution transmission electron microscopy (HRTEM) was conducted using field emission TEM (JEM-2100F; JEOL) to observe the morphology and primary particle size. The beam was scanned across the samples. Then selected-area electron diffraction (SAED) patterns were taken from sample area of about 100 nm. Synchrotron X-ray total scattering experiments were conducted at beamline 8B of the Photon Factory KEK, Tsukuba, Japan. An incident X-ray beam was monochromatized using a Si(111) double-crystal monochromator to the wavelength of 0.61921(1) Å, which was calibrated with a CeO_2 powder diffraction pattern. The monochromatic beam was doubly focused using a cylindrical Rh-coated bent-focusing mirror. The focal spot size was approximately 0.5 mm horizontal by 0.3 mm vertical. The samples were loaded in 0.7 mm Lindemann glass capillaries. Data were recorded on a large Debye–Scherrer camera with radius of 191.3 mm equipped with a curved imaging plate detector at angles of up to 145^o corresponding to Q_{max} = 20 $Å^{-1}$. The X-ray exposure time for each sample was 60 min. The glass capillary was rotated continuously about the φ-axis through 180^o during exposure. The two-dimensional diffraction images were integrated as a function of 2θ using software (DISPLAY; Rigaku Corp.). The data were entered into the PDFGetX2 program [24], which was used to make corrections for background scattering, sample absorption, X-ray polarization, Compton scattering, and normalization by average atomic scattering power. The Fourier transform of the data yielded the atomic pair distribution function: G(r). PDF fitting was attempted using PDFgui [25], with a view to confirming the structure parameters and to estimating an accurate average primary particle size for each sample. The starting atomic coordinates for the 6-line ferrihydrite were taken from the atomic position of the Fhyd3 determined by Michel et al. [13]. The isotropic

temperature factors and site occupancy factors were fixed at the values of the Fhyd3 during refinements.

3 Results

Figure 1 shows changes of the synchrotron X-ray diffraction patterns as a function of heating time. The XRD pattern at heating time of 10 min displays a typical diffraction profile of the 6-line ferrihydrite which comprises six major peaks. No other phase was detected. At heating time of 4 h, new diffraction peaks belonging to hematite (α-Fe_2O_3) start to be observed on the XRD profile. The peaks strengthen and sharpen during the heating time of 4 h. Hematite is the only crystalline phase formed from the ferrihydrite during the experiment.

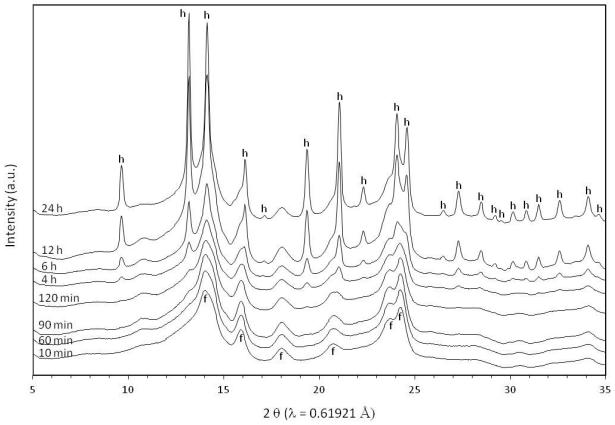

Fig 1 Synchrotron X-ray diffraction patterns showing the change from 6-line ferrihydrite to hematite.

Figure 2 presents HRTEM images and SAED patterns of the samples obtained from the different heating times. Nanodiffraction patterns can be indexed, and individual diffractions are identifiable using angles and ratios of spacings between spots.

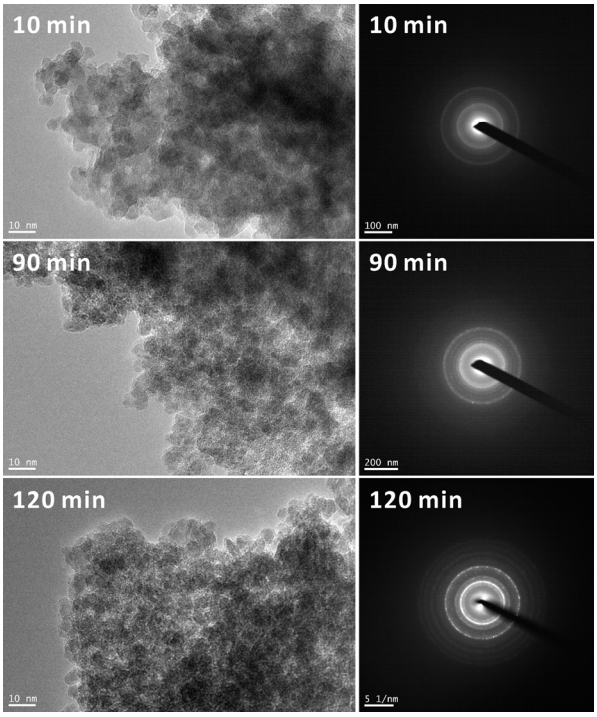

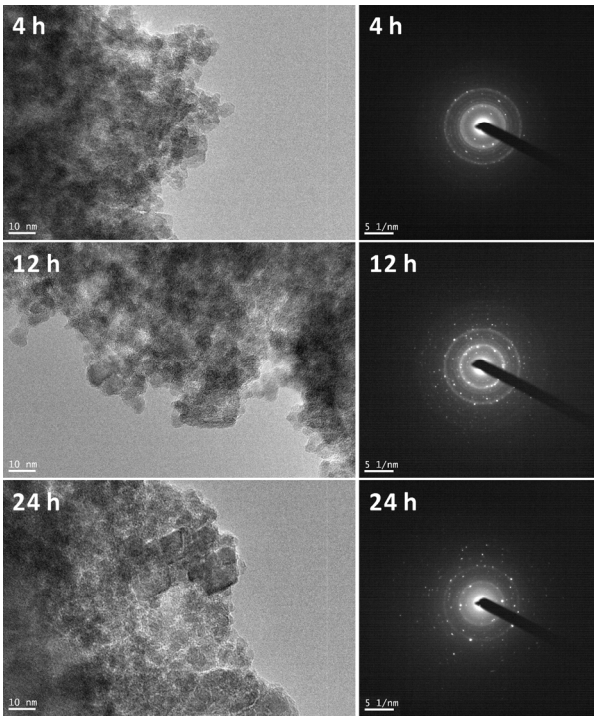

Fig 2 HRTEM images and SAED patterns of samples of heating time from 10 min to 24 h.

The SAED patterns of the samples with heating times of 10–120 min exhibit broadly diffuse Debye rings corresponding to those of the 6-line ferrihydrite. They show complete agreement with those described for the 6LFh sample by Janney et al. [26]. The SAED pattern from the sample of heating time of 4 h, however, displays two clear diffraction spots inside the first Debye ring from the ferrihydrite. They can be indexed to the (012) diffraction plane from hematite. Diffraction spots resulting from hematite strengthener are clearly visible, increasing with heating time greater than 4 h. The SAED patterns change to rather spotty Debye rings with no additional diffraction ring. Results of the SAED observations are entirely consistent with those of XRD measurements in this study. From TEM images, however, ascertaining the edges of aggregates consisting of individual crystallites is difficult. Furthermore, a long time is necessary to count a sufficient number of nanoparticles for accurate determination of size and size distribution. Therefore, it is difficult to examine the accurate size of nanoparticles using TEM. The nanoparticles size can nevertheless be estimated roughly by considering the error based on the standard deviations of particle size distribution. The HRTEM image from the sample of heating time of 10 min shows that most particles are approximately 5 nm, but individual sizes range widely: 3–10 nm (Figure 2). Most particles are rounded, showing mutual aggregation. Despite the increased heating time, the crystallite sizes seem to remain unchanged. Although the SAED pattern from the sample of heating time of 4 h shows diffraction spots from hematite, the particle size is almost constant. The particle size, however, starts to grow gradually after the heating time of 12 h. At heating time of 24 h, the edges of

aggregates become indistinct compared to those of previous samples. In addition, several large particles display straight edges and angular shapes with length greater than 10 nm. The rhombohedral shape of hematite nanocrystals shows good agreement with those reported recently by Echigo et al. [27].

The synchrotron X-ray total scattering data obtained from samples obtained with heating times of 10, 60, 90, 120 min, and 4 h were used to investigate structural changes in ferrihydrite, especially a phase transformation mechanism of the 6-line ferrihydrite to hematite. Figure 3 shows variations of the atomic PDF patterns as a function of the heating time.

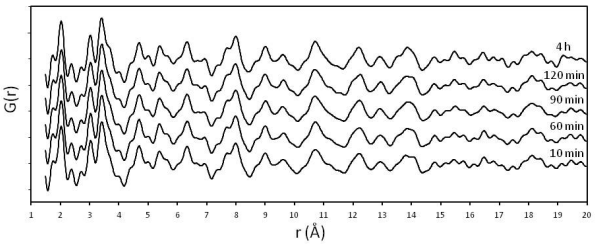

Fig 3 PDF patterns showing the local structural change on transformation from 6-line ferrihydrite to hematite.

The dry thermal transformation of 2-line ferrihydrite to hematite was investigated using the atomic PDF method [9]. The local structural changes on transformation from the 2-line ferrihydrite to hematite are observed as a shoulder at 3.655 Å on the PDF pattern. That shoulder corresponds to the structural distortions caused by Fe–Fe distance change between corner-sharing FeO_6 octahedra [9]. In the present study, this subtle change at 3.6 Å is also visible (Figure 3). To refine the crystal structure model directly and to obtain quantitative estimates of the average particle size, the PDF patterns were fitted with the reported ferrihydrite structure [13] using the PDFgui program [25]. Figure 4 shows the measured and calculated PDFs from the sample of heating time of 10 min along with the residual data. The fitting quality is apparently adequate to verify the produced parameters. The final R factors for ferrihydrite are 20–30% at the smallest because the fitting is reflected by occurrences of surface relaxation, internal strain, and stacking faults at the particle surface [13].

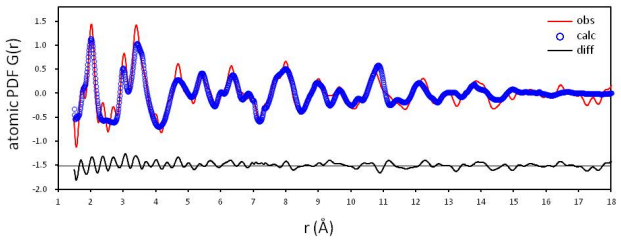

Fig 4 Observed and calculated PDFs, and the residual values obtained from sample of heating time of 10 min.

4 Discussion

Structural changes with particle size

The particle size of the 6-line ferrihydrite estimated from attenuation of the PDF varies from 28 to 35 Å. This estimation is distinctly smaller than the results of HRTEM observation. According to an earlier report [13], however, the coherent scattering domain size of 6-line ferrihydrite (Fhyd3) as estimated using the PDF method is about 3 nm, which is slightly smaller than that estimated from HRTEM analysis. Therefore, the particle sizes estimated using the PDF method have a smaller value than the value observed directly using HRTEM analysis. Figure 5 provides evolutions of the unit-cell parameters of the 6-line ferrihydrite as a function of particle size.

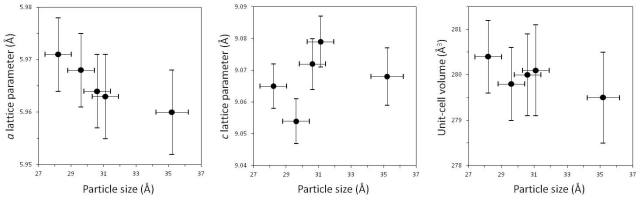

Fig 5 Plots of unit-cell parameters *a*, *c*, and *V* as functions of particle size.

The *c* lattice parameter shows no clear dependence on the particle size, although a strong tendency is apparent in the ferrihydrite structure to decrease the *a* lattice parameter with increasing particle size, which is attributed to the decrease of the unit-cell volume (Figure 5). The decreasing particle size is well known to increase the surface free energy of particles. Therefore, it is readily apparent that the decreasing particle size is accompanied by the increasing unit cell volume.

The bond distances and angles in three coordination polyhedra: $Fe(1)O_6$, $Fe(2)O_6$, and $Fe(3)O_4$ are refined, but no definite trend is apparent between particle size and bond distances. The variations of the coordination polyhedral parameters are shown in Figure 6.

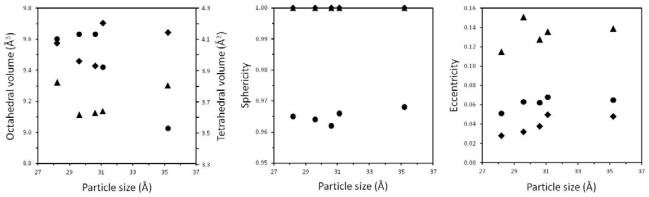

Fig 6 Plots of coordination polyhedral parameters as functions of particle size. The $Fe(1)O_6$ octahedron, $Fe(2)O_6$ octahedron, and $Fe(3)O_4$ tetrahedron are represented by filled circles, diamonds, and triangles, respectively.

The volume of $Fe(1)O_6$ octahedron is decreased with the particle size, whereas those of $Fe(2)O_6$ octahedron and $Fe(3)O_4$ tetrahedron show no clear particle size dependence. The parameters of sphericity and eccentricity indicate a degree of polyhedral distortion and variations of ligand positions. The distortions and morphologies of three coordination polyhedra, however, remain constant under a continuous decrease of the *a* lattice parameter.

Phase transformation mechanism of ferrihydrite to hematite

Under the experimental conditions examined in the study, a linear relationship exists between the *a* lattice parameter and the particle size. Figure 7 shows the difference of crystal structure between ferrihydrite and hematite. The crystal structure of ferrihydrite [13]

comprises two kinds of sheets parallel to *c* axis: one is a six-membered ring made of six FeO_6 octahedra (A sheet); another is a six-membered ring made of three FeO_6 octahedra and three FeO_4 tetrahedra (B sheet). In contrast, that of hematite comprises sheets of six-membered rings made of FeO_6 octahedra (A sheet) parallel to *c* axis.

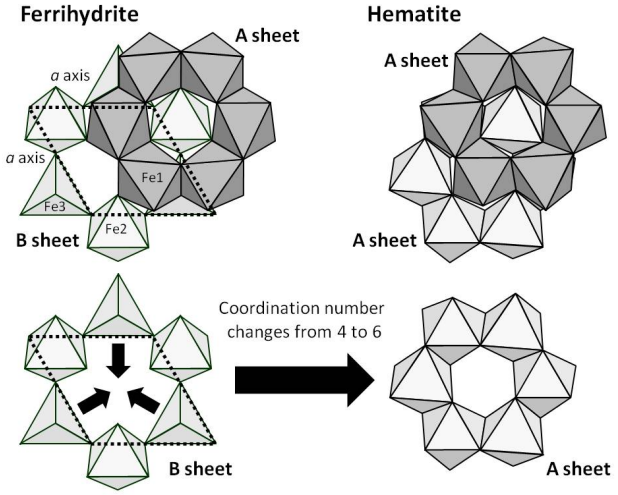

Fig 7 Crystal structures of ferrihydrite and hematite viewed down [001]. Phase transformation from ferrihydrite to hematite occurs when the tetrahedral coordination in the B sheet changes into octahedral coordination with contraction.

As the particle size increases, contractions of the six-membered rings in ferrihydrite are caused by decreasing the *a* lattice parameter. When the B sheet is contracted continuously and the local neighborhoods of the coordinating ligands are brought mutually closer, the coordination environment of the Fe(3) atom must be changed from tetrahedral to octahedral (Figure 7). Consequently, the B sheet can be transformed into an A sheet with increasing particle size. Because the B sheet changes into the A sheet, which is the same configuration of hematite, ferrihydrite transforms into hematite with increasing particle size. When the particle size of ferrihydrite is 28 Å, the diagonal distance across the A sheet is 4.44 Å. As the particle size increases, this diagonal distance also decreases monotonously. Through phase transformation of ferrihydrite to hematite, the diagonal distance between two opposing oxygen atoms in hematite becomes 4.19 Å.

In numerous structures, geometrical changes upon cooling from high temperatures are similar to those upon compression: structural variations caused by changes in temperature might be offset by variations attributable to the change in pressure (Figure 8).

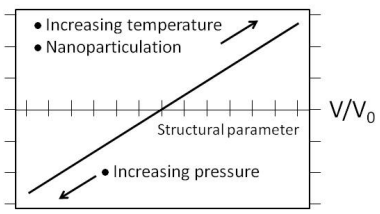

Fig 8 Idealized inverse effects of temperature, pressure, and nanoparticulation on structure.

This relation has been called an "inverse relationship" [28]. Considering this inverse relationship, the structural change with decreasing particle size (nanoparticulation) is fundamentally similar to that which occurs with increasing temperature (Figure 8).

Acknowledgement

The authors would like to thank Prof. Kumai and the beamline staffs for great support during the powder XRD experiments. This work was supported by a Grant-in-Aid for Young Scientists (B) from the Japan Society for the Promotion of Science (project no. 24740352). This work was also supported in part by the Nanotechnology Platform Japan Program of the Ministry of Education, Culture, Sports, Science and Technology of Japan.

References

[1] U. Schwertmann and R.M. Cornell, Iron oxides in the laboratory: preparation and characterization. *Wiley-VCH*, New York (2000).
[2] M.M. Benjamin, *J. Coll. Interf. Sci.* **79**, 209 (1981).
[3] K.P. Raven *et al, Env. Sci. Tech.* **32**, 344 (1998).
[4] J.G. Webster et al., *Env. Sci. Tech.* **32**, 1361 (1998).
[5] A. Jain *et al., Env. Sci. Tech.* **33**, 1179 (1999).
[6] E. Liger *et al., Geo. Cosm. Acta* **63**, 2939 (1999).
[7] U. Schwertmann et al., *J. Coll. Inter. Sci.* **209**, 215 (1999).
[8] D.J. Burleson and R.L. Penn, *Langmuir* **22**, 402 (2006).
[9] W. Xu et al., *Am. Mineral.* **96**, 513 (2011).
[10] V.A. Drits *et al.,* Clay Mineral. **28**, 185 (1993).
[11] J.L. Jambor and J.E. Dutrizac, *Chem. Rev.* **98**, 2549 (1998).
[12] E. Jansen *et al., Appl. Phys*. **A74**, S1004 (2002).
[13] F.M. Michel *et al., Science* **316**, 1726 (2007).
[14] D.G. Rancourt and J.F. Meunier *Am. Mineral.* **93**, 1412 (2008).
[15] A. Manceau *Clay Mineral.* **44**, 19 (2009).
[16] F.M. Michel *et al., Proc. Nat. Acad. Sci.* **107**, 2787 (2010).
[17] A. Manceau *Clay Mineral.* **45**, 225 (2010).
[18] A. Manceau *Am. Mineral.* **96**, 521 (2011).
[19] A. Manceau *Env. Sci. Tech.* **46**, 6882 (2012).
[20] V. Barron *et al., Am. Mineral*. 97, 253 (2012).
[21] F. Maillot et al., *Geo. Cosm. Acta* **75**, 2708 (2011).
[22] C. Mikutta. *Geo. Cosm. Acta* **75**, 5122 (2011).
[23] D. Peak and T. *Env. Sci. Tech.* **46**, 3163 (2012).
[24] X. Qiu et al., *J. Appl. Cryst.* **37**, 678 (2004).
[25] C.L. Farrow *et al., J Phys. Cond. Mat.* **19**, 335219 (2007).
[26] D.E. Janney *et al., Clays Clay Min.* **48**,111 (2000).
[27] T. Echigo et al., *Geo. Cosm. Acta*. **90**, 149 (2012).
[28] R.M. Hazen and L.W. Finger, Comparative crystal chemistry: temperature, pressure, composition and the variation of crystal structure. *John Wiley & Sons,* New York, (1982)

* kyono@geol.tsukuba.ac.jp